



Exploring the Properties of the Electron Strahl at 1 AU as an Indicator of the Quality of the Magnetic Connection Between the Earth and the Sun

Joseph E. Borovsky*

Center for Space Plasma Physics, Space Science Institute, Boulder, CO, United States

OPEN ACCESS

Edited by:

Daniele Telloni,
National Institute of Astrophysics
(INAF), Italy

Reviewed by:

Daniel Verscharen,
University College London,
United Kingdom
Allan Macneil,
University of Reading, United Kingdom
Curt A. De Koning,
University of Colorado, Boulder, CO,
United States

*Correspondence:

Joseph E. Borovsky
jborovsky@spacescience.org

Specialty section:

This article was submitted to
Space Physics,
a section of the journal
Frontiers in Astronomy and
Space Sciences

Received: 26 December 2020

Accepted: 29 January 2021

Published: 05 March 2021

Citation:

Borovsky JE (2021) Exploring the Properties of the Electron Strahl at 1 AU as an Indicator of the Quality of the Magnetic Connection Between the Earth and the Sun. *Front. Astron. Space Sci.* 8:646443. doi: 10.3389/fspas.2021.646443

In this report some properties of the electron strahl at 1 AU are examined to assess the strahl at 272 eV as an indicator of the quality of the magnetic connection of the near-Earth solar wind to the Sun. The absence of a strahl has been taken to represent either a lack of magnetic connection to the corona or the strahl not surviving to 1 AU owing to scattering. Solar-energetic-electron (SEE) events can be used as indicators of good magnetic connection: examination of 216 impulsive SEE events finds that they are all characterized by strong strahls. The strahl intensity at 1 AU is statistically examined for various types of solar-wind plasma: it is found that the strahl is characteristically weak in sector-reversal-region plasma. In sector-reversal-region plasma and other slow wind, temporal changes in the strahl intensity at 1 AU are examined with 64 s resolution measurements and the statistical relationships of strahl changes to simultaneous plasma-property changes are established. The strahl-intensity changes are co-located with current sheets (directional discontinuities) with strong changes in the magnetic-field direction. The strahl-intensity changes at 1 AU are positively correlated with changes in the proton specific entropy, the proton temperature, and the magnetic-field strength; the strahl-intensity changes are anti-correlated with changes in the proton number density, the angle of the magnetic field with respect to the Parker-spiral direction, and the alpha-to-proton number-density ratio. Reductions in the strahl intensity are not consistent with expectations for a simple model of whistler-turbulence scattering. Reductions in the strahl intensity are mildly consistent with expectations for Coulomb scattering, however the strongest-observed plasma-change correlations are unrelated to Coulomb scattering and whistler scattering. The implications of the strahl-intensity-change analysis are that the change in the magnetic-field direction at a strahl change represents a change in the magnetic connection to the corona, resulting in a different strahl intensity and different plasma properties. An outstanding question is: Does an absence of an electron strahl represent a magnetic disconnection from the Sun or a poor strahl source in some region of the corona?

Keywords: solar wind, heliosphere, corona, strahl, space weather

INTRODUCTION

Knowing the magnetic connectivity between the Earth and the Sun is desirable for several reasons: e.g., 1) to gain a global understanding of the heliospheric magnetic structure, (e.g. McComas et al., 1989; Crooker et al., 2002; Crooker and Pagel, 2008; Crooker and Owens, 2012; Lockwood, 2013; Viall and Borovsky, 2020), 2) for understanding solar energetic particle (proton and electron) events and particle transport (Mazur et al., 2000; Chollet and Giacalone, 2011; Trenchi et al., 2013), and 3) for assessing the likelihood that Earth will or will not undergo an energetic-particle event.

One promising method to assess the magnetic connectivity between the near-Earth solar wind and the Sun is to interpret observations of the electron strahl in the near-Earth solar wind. The electron strahl is a beam of magnetic-field-aligned electrons originating from the solar corona that propagate away from the Sun (Feldman et al., 1976; Pilipp et al., 1987; Maksimovic et al., 2005). A robust strahl is a signature of a good magnetic connection to the Sun; an absence of a strahl has been historically interpreted as an indication of either 1) no magnetic connection to the Sun (McComas et al., 1989; Gosling et al., 2005) or 2) a strahl that does not survive from the Sun to the observer (Pagel et al., 2005a; Crooker and Pagel, 2008; Chollet et al., 2010).

In the present study the intensity of the electron strahl at 272 eV is measured. Lin and Kahler (1992) examined a number of events that were judged to be magnetic-disconnection events by an absence of a low-energy strahl and found the presence of higher-energy (2 keV–8.5 keV) strahls, calling into question whether the absence of a lower-energy strahl is an indication of a magnetic disconnection from the Sun. However, Gosling et al., (2005) examined cases of reconnection-exhaust magnetic disconnections and found that electron-halo intermixing could give the impression of a higher-energy strahl, even though those magnetic-field lines were definitely disconnected from the Sun (See also the analysis of Crooker and Pagel (2008)).

At a distance of 1 AU from the Sun, the intensity of the electron strahl varies on multiple timescales, with sudden jumps in strahl intensity that are observed to be co-located with strong current sheets (magnetic directional discontinuities) (Gosling et al., 2004a; Borovsky, 2020a,b). Hence, temporal jumps in the strahl intensity are associated with sudden changes in the magnetic-field orientation.

This report explores some properties of the electron strahl that impact the ability to assess the magnetic connection between Earth and the Sun using observations of the strahl in the near-Earth solar wind. In **The Electron Strahl and the Types of Solar Wind Plasma** the relationship of the strahl intensity to the type of solar-wind plasma is investigated. In **Impulsive SEE Events, the Electron Strahl, and the Type of Plasma** the intensity of the electron strahl at 1 AU is examined during impulsive solar-energetic-electron (SEE) events, which are times when there must be a good magnetic connection between the Earth and the Sun. In **Strahl Analysis** sudden changes in the intensity of the electron strahl at 1 AU are statistically examined in relation to sudden changes in other plasma parameters and the statistical

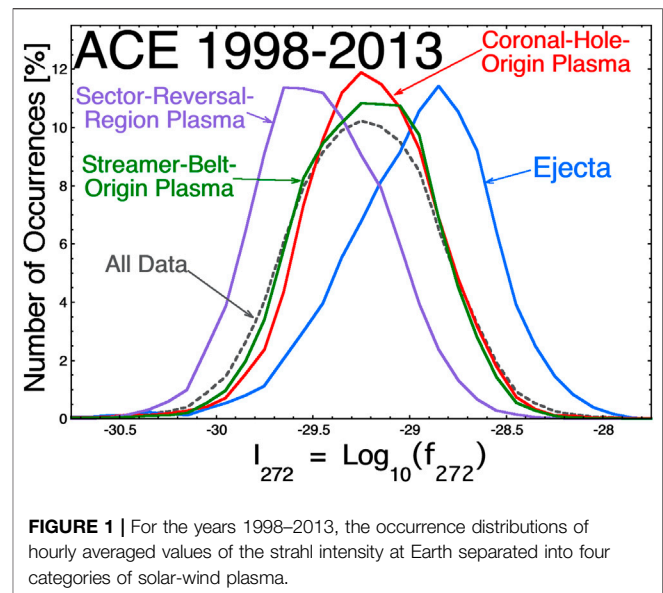


FIGURE 1 | For the years 1998–2013, the occurrence distributions of hourly averaged values of the strahl intensity at Earth separated into four categories of solar-wind plasma.

results are discussed in relation to ideas about strahl destruction by Coloumb scattering and whistler-turbulence scattering are tested. **Discussion: Interpretation of Strahl-Intensity Changes, Assessing the Sun-Earth Connection, and the Future** contains discussions of 1) the interpretations of strahl-intensity changes, 2) an assessment of the ability to determine the Sun-Earth magnetic connection, and 3) suggestions for future research.

THE ELECTRON STRAHL AND THE TYPES OF SOLAR WIND PLASMA

Various types of solar-wind plasma are emitted into the heliosphere from various types of regions on the rotating Sun. These various types of plasma have systematically differing parameters at 1 AU, (e.g. proton specific entropy, speed, heavy-ion charge-state ratios, Alfvén velocity, etc.), which allows the solar wind to be categorized into the various types of plasmas (cf. Neugebauer et al., 2003, 2016; Reisenfeld et al., 2003; Zhao et al., 2009; Xu and Borovsky, 2015; Camporeale et al., 2017; Veselovsky et al., 2018; Li et al., 2020; Amaya et al., 2020; Heidrich-Meisner et al., 2020; Bloch et al., 2020). One characteristic difference between the various types of plasma at 1 AU is the intensity of the electron strahl (Borovsky, 2018). In **Figure 1** the hourly averaged intensity of the electron strahl as measured by the SWEPAM instrument (McComas et al., 1998) on the ACE spacecraft at L1 upstream of the Earth is binned for the four types of solar-wind plasma in the Xu and Borovsky (2015) plasma-categorization scheme. I_{272} is the base-10 logarithm of the phase-space density f_{272} (in units of s^2cm^{-5}) of the electron strahl in the dominant (parallel-to- \mathbf{B} or antiparallel-to- \mathbf{B}) direction at an energy of 272 eV, as measured by ACE SWEPAM (See Borovsky, (2017) for a discussion of the creation of an hourly averaged index of I_{272}). In **Figure 1** the gray dashed curve is the occurrence distribution of the hourly averaged strahl intensity I_{272} for all

data in the years 1998–2013. The other four curves in **Figure 1** are the occurrence distributions of hourly averaged strahl intensity in four types of solar-wind plasma: coronal-hole-origin plasma (red), streamer-belt-origin plasma (green), sector-reversal-region plasma (purple), and ejecta (blue). Ejecta plasma (blue) has a systematically more-intense strahl and sector-reversal-region plasma (purple) has a systematically weaker strahl, with coronal-hole-origin plasma (red) and streamer-belt-origin plasma (green) have more-typical values of the strahl intensity.

Because of the robust strahl intensities in **Figure 1**, (e.g. greater than ~ -29.75), it can be assumed that coronal-hole-origin, streamer-belt-origin, and ejecta plasmas at 1 AU are, in general, well connected magnetically to the Sun. This can't be assumed for sector-reversal-region plasmas, which has a range of strahl intensities in **Figure 1** that can be quite weak, (e.g. less than -29.75). Two sources of sector-reversal-region plasma are discussed in the literature. The first is disconnection of magnetic field caused by reconnection between open flux on either side of a streamer stalk (Wang et al., 1999; Sanchez-Diaz et al., 2019; Lavraud et al., 2020), resulting in the emission of blobs of plasma in the streamer-stalk region. Disconnections will certainly result in a decreased strahl intensity. The second source is interchange reconnection between open field lines and closed loops of streamers (Wang et al., 2000; Crooker et al., 2004; Rouillard et al., 2020). Individual interchange reconnection events, which change the magnetic connection into loops of different heights and electron temperatures, will almost certainly result in a change in the strahl intensity. Sector-reversal-region plasma contains such features as streamer-stalk blobs and puffs (Wang et al., 2000; Bemporad et al., 2005; Sheeley et al., 2009; Rouillard et al., 2010; Sheeley and Rouillard, 2010; Foullon et al., 2011) and periodic density structures (Viall et al., 2010; Viall and Vourlidis, 2015) that are of interest for their impact on Earth (Kepko and Spence, 2003; Viall et al., 2009; Kepko and Viall, 2019). These plasma structures in the sector-reversal-region plasma can be associated with magnetic disconnections from the Sun (Wang et al., 1999; Kepko et al., 2016). There are also reconnection-disconnection events in the vicinity of the heliospheric current sheet in the sector-reversal-region plasma, (e.g. Gosling et al., 2005; Lavraud et al., 2009, 2020; Sanchez-Diaz et al., 2019). Based on the weaker strahl, streamer-belt-origin plasma is the most likely solar-wind type to be poorly connected to the Sun.

Another possible indicator of magnetic connection to the Sun is whether or not the magnetic-field in a plasma has a Parker-spiral orientation. Plasma that is steadily emitted from a spot on the Sun will have an approximately Parker-spiral oriented magnetic field (Parker, 1958; Fisk, 2001; Georgieva et al., 2005); plasma that is impulsively emitted, which can include magnetic disconnections, need not have a Parker-spiral-oriented magnetic field. Even for steadily emitted solar wind, there can be underwinding, (e.g. Gosling and Skoug, 2002; Murphy et al., 2002; Riley and Gosling, 2007) or overwinding, (e.g. Smith and Bieber, 1991; Bruno and Bavassano, 1997) of the Parker spiral caused by large-scale compressions and rarefactions, and there are always large fluctuations of the magnetic-field direction about the Parker-spiral direction (Ness and Wilcox, 1966; Forsyth et al.,

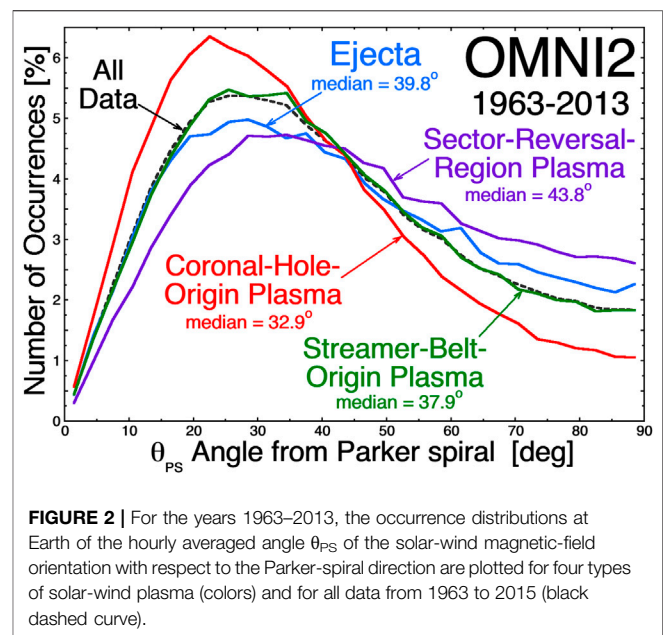


FIGURE 2 | For the years 1963–2013, the occurrence distributions at Earth of the hourly averaged angle θ_{PS} of the solar-wind magnetic-field orientation with respect to the Parker-spiral direction are plotted for four types of solar-wind plasma (colors) and for all data from 1963 to 2015 (black dashed curve).

1996; Burlaga and Ness, 1997; Borovsky, 2010). In **Figure 2** the hourly averaged angle between the magnetic-field-line orientation in the solar wind at Earth and the Parker-spiral direction is binned, with the Parker-spiral direction calculated every hour using the hourly averaged speed of the solar wind (This field-line orientation does not account for the sign of \mathbf{B} nor does it consider the sign of \mathbf{B} relative to the toward or away sector structure.) The OMNI data set (King and Papitashvili, 2005) for the years 1963–2013 was used. In **Figure 2** the distribution of coronal-hole-origin values (red curve) is the most Parker-spiral aligned and the distribution of sector-reversal-region values (purple curve) is the least Parker-spiral aligned. Note that owing to fluctuations in the direction of the magnetic field about the mean Parker-spiral direction, the instantaneous magnetic-field direction (and the hourly averaged field direction) is rarely exactly Parker-spiral aligned (Borovsky, 2010). The facts 1) that the magnetic field is less-Parker-spiral oriented in sector-reversal-region plasma and 2) that the strahl intensity is less intense in sector-reversal-region plasma enforce the notion that the strahl intensity and the field orientation can be indicators of good or poor magnetic connection to the Sun. As will be seen in **Strahl Analysis**, the strahl intensity and the angle of the magnetic field from the Parker spiral are weakly anti-correlated in the solar wind at 1 AU.

IMPULSIVE SEE EVENTS, THE ELECTRON STRAHL, AND THE TYPE OF PLASMA

Impulsive solar energetic electron (SEE) events at 1 AU are associated with solar x-ray flares, (e.g. Kallenrode and Svestka, 1994; Cliver and Ling, 2007) or near-Sun events (Li et al., 2013) and electrons accelerated near the Sun traveling along the solar-wind magnetic field out to a measuring spacecraft at 1 AU. If one

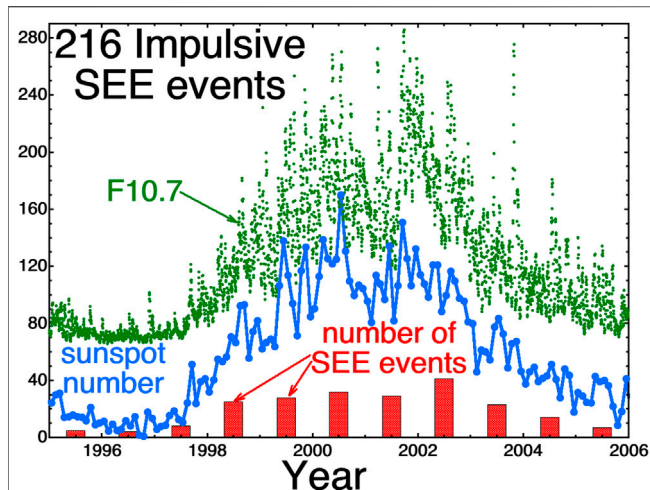


FIGURE 3 | For 216 impulsive SEE events from the Wang et al., (2012) catalog, the number of events per year is plotted as the red bars. Also plotted is the monthly sunspot number (blue) and the daily averaged value of F10.7 (green).

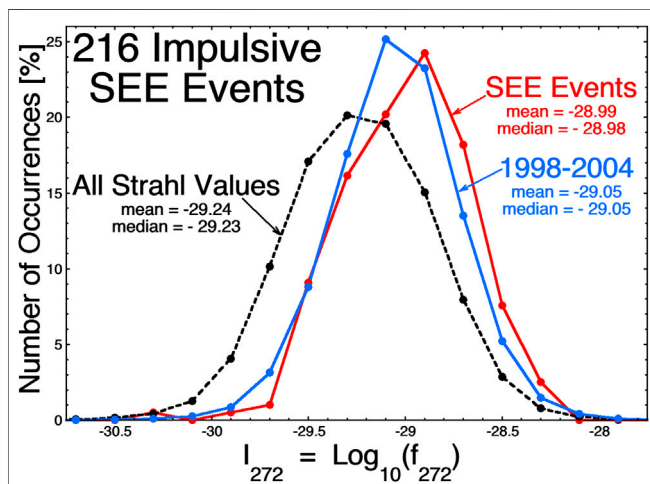


FIGURE 4 | For the 216 impulsive SEE events, the distribution of strahl intensities is plotted (red curve). Also plotted is the occurrence distribution of hourly averaged strahl intensities in the 1998–2004 solar maximum (blue curve) and for the years 1998–2013 (black dashed curve).

can assume that impulsive SEE events are good indicators of magnetic connectivity to the Sun, then examining the strahl intensity during the early times in impulsive SEE events vs. the strahl intensity when SEE events are not seen could be a test of the viability of using the strahl intensity as a gauge of magnetic connectivity to the Sun. Good connectivity to the Sun may be a valid assumption for impulsive SEE events (cf. Figure 2.3b of Reames (1999)) or it might not be a valid assumption (cf. Figure 6 of Wibberenz and Cane (2006)).

Assuming SEE events are well connected to the Sun at early times, to explore other conditions of good magnetic connection 216 impulsive SEE events from the near-Earth catalog of Wang

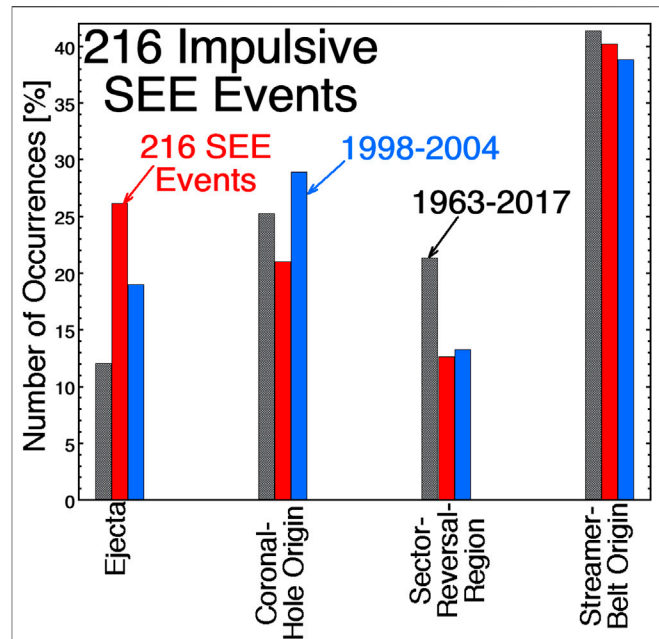


FIGURE 5 | The occurrence distribution of the type of solar-wind plasma that the Earth is in when 216 impulsive SEE events occurred is plotted as the red bars (middle). The occurrence distributions of the type of solar-wind plasma the Earth is in are also plotted for the solar-maximum years 1998–2004 (blue, right) and for the years 1963–2017 (black, left).

et al., (2012) are used: specifically, the 216 events in the catalog that had peak electron kinetic energies of 310 keV or higher.

In **Figure 3** the distribution of the 216 SEE events vs. time is plotted as the red bars, along with the monthly sunspot number (blue) and the daily averaged F10.7 flux (green). As could be expected, since the SEE events are associated with solar flares, the occurrence of the SEE events is concentrated during solar maximum.

In **Figure 4** the occurrence distribution of electron-strahl intensities at Earth during the 216 SEE events is plotted as the red curve using hourly averaged values of the strahl intensities from ACE SWEPAM. The black dashed curve plots the distribution of strahl intensities for the years 1998–2013 and the blue curve plots the distribution for the solar-maximum interval 1998–2004 (which is also plotted in **Figure 1**). Hence, it is probably not the case that there are SEE events at Earth that are missed because the Earth was not magnetically connected to the Sun: it would appear that the Earth tends to have good magnetic connections during solar maximum. As can be seen in **Figure 4** the strahl intensities for the 216 SEE events are robust in comparison with the black distribution for all times during the years 1998–2013. One might think that the electron strahl should be intense when solar energetic electrons are present because they are two energies out of the same electron distribution function, but that is not the case: the strahl is a representation of the coronal electron temperature (Bercic et al., 2020; Boldyrev et al., 2020) and the solar energetic electrons are produced by specific temporal acceleration processes (Kallenrode and Svestka, 1994; Cliver and Ling, 2007; Li et al., 2013). Also, for the early times of impulsive SSE events, the 272 eV electrons of the observed strahl at 1 AU left the Sun more than 4.3 h before the flare occurred.

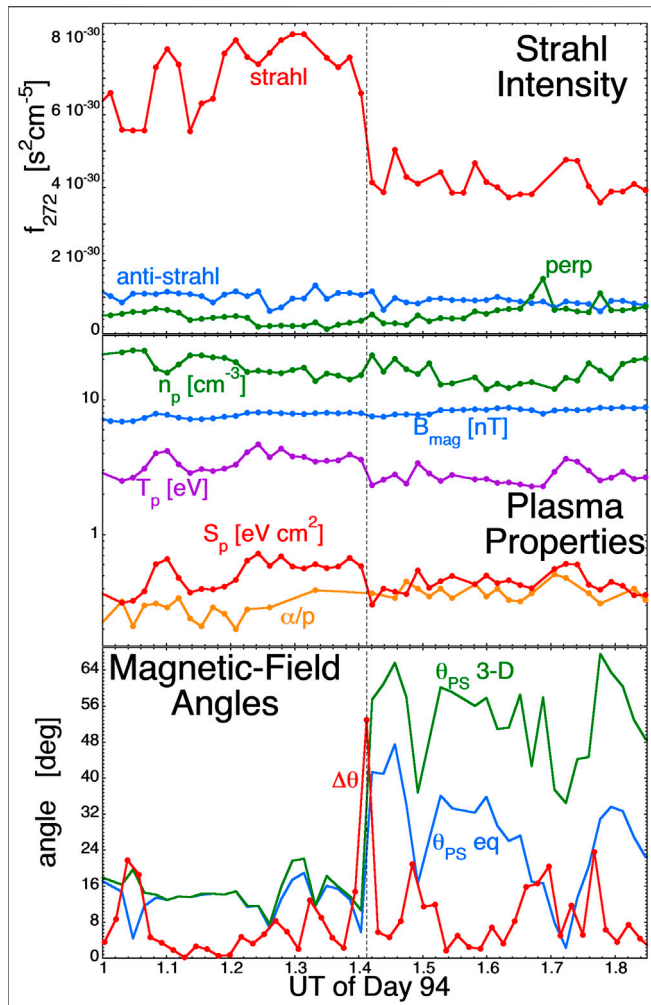


FIGURE 6 | An example of a sudden decrease in the strahl intensity (marked by the vertical dashed line) on April 5, 2005.51 min of 64-s-resolution measurements by the instruments on ACE at L1 are plotted. The quantities plotted are described in the text.

Using the Xu and Borovsky (2015) categorization scheme, the type of solar-wind plasma that the Earth is in when each of the 216 SEE events were seen is binned as the red bars in Figure 5; also binned is the plasma categorization for the 1998–2004 solar maximum interval (blue bars, right) and for the entire 1963–2017 OMNI2 solar-wind data base (black bars, left). With poor statistics having divided the 216 SEE events into four bins, the occurrence distribution of plasma types for the 216 SEE events (red) is not inconsistent with the occurrence distribution of plasma types for solar maximum (blue): the SEE occurrence distribution is a little higher on ejecta and a little lower on coronal-hole-origin plasma.

STRAHL ANALYSIS

Magnetic disconnections from the Sun have been indicated by heat-flux dropouts (an absence of an electron strahl), although it has been argued that not all heat-flux dropouts are magnetic

disconnections (cf. Lin and Kahler, 1992; Pagel et al., 2005a; Crooker and Pagel, 2008; Chollet et al., 2010). It is of interest to interpret whether the presence or absence of an electron strahl at 1 AU indicates the presence or absence of a magnetic connection to the Sun, or whether the absence of a strahl is caused by the scattering of the strahl between the Sun and 1 AU. To inform this, sudden changes in the intensity of the electron strahl at 1 AU are examined and compared with other simultaneous changes to determine whether the strahl-intensity changes at 1 AU might be associated with changes in the amount of strahl scattering. In the present study the focus of the strahl-change analysis will be on sector-reversal-region plasma with its generally weak strahl intensity; changes of strahl intensity in fast solar wind, (i.e. coronal-hole-origin plasma), (e.g. Hammond et al., 1996; Pagel et al., 2005b; Louarn et al., 2009; Borovsky, 2016) where the strahl intensity stays robust (cf. Figure 1), indicating always a magnetic connection to the corona, are not examined since those variations may not provide information about magnetic disconnections (A

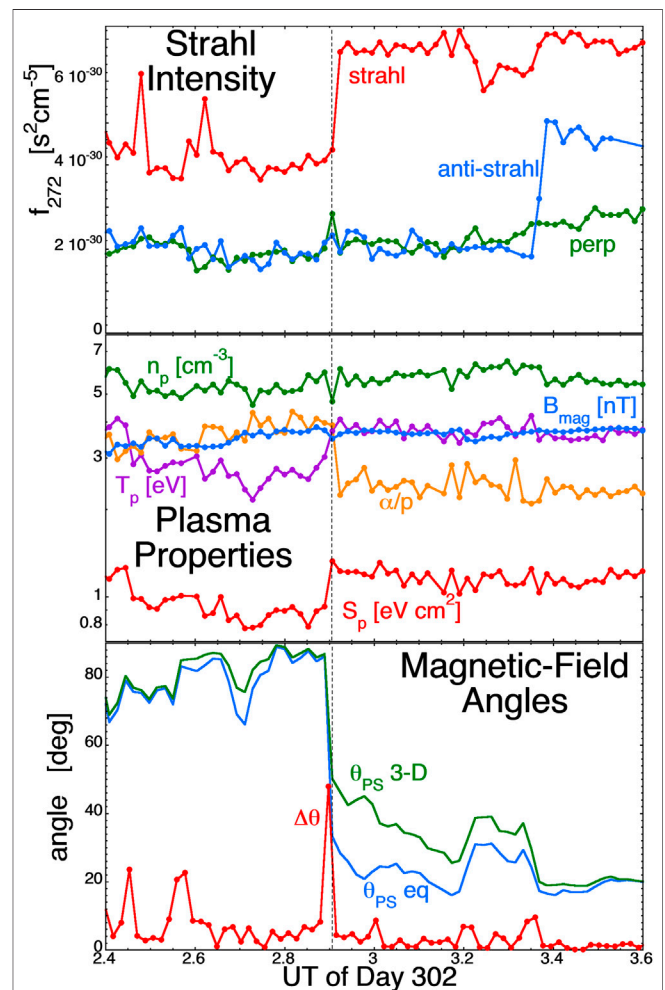


FIGURE 7 | An example of a sudden increase in the strahl intensity (marked by the vertical dashed line) on October 29, 2005.72 min of 64-s-resolution measurements by the instruments on ACE at L1 are plotted. The quantities plotted are described in the text.

future study of the strahl-intensity changes in the coronal-hole-origin solar wind could, however, provide additional information about how to interpret strahl changes.)

Using the 64-sec-resolution ACE plasma SWEPAM and magnetic-field MAG (Smith et al., 1998) data at L1, two examples of strahl changes appear in **Figures 6** and **7**. The first change, in **Figure 6**, was a sudden decrease in the strahl intensity at ACE at 1:24 UT on April 4 (Day 94) of 2005. In the top panel the strahl phase space density f_{272} at 272 eV is plotted in red, the phase-space density in the opposite direction (anti-strahl) is plotted in blue, and the electron phase-space density at 272 eV perpendicular to the magnetic-field direction is plotted in green. The drop in strahl intensity by a factor of about two is denoted by the vertical black dashed line. In the middle panel of **Figure 6** a number of plasma parameters are plotted: the proton number density n_p (green), the proton temperature T_p (purple), the proton specific entropy $S_p = T_p/n_p^{2/3}$ (red), the alpha-to-proton number-density ratio α/p (orange), and magnetic-field strength B_{mag} (blue). Note that simultaneously for this drop in the strahl intensity there is a drop in the proton specific entropy S_p and a drop in the proton temperature T_p . In the bottom panel of **Figure 6** some information about the direction of the solar-wind magnetic field is plotted: $\Delta\theta$ (red) is the angular change in the magnetic-field direction every 64 s, $\theta_{\text{PS } 3\text{-D}}$ (green) is the angle between the magnetic field and the Parker-spiral direction, and $\theta_{\text{PS eq}}$ (blue) is the angle between the equatorial projection of the magnetic field and the Parker-spiral direction. A large value of $\Delta\theta$ is an indication of a crossing of a strong current sheet: as can be seen in the plot of $\Delta\theta$, there is a strong current sheet co-located with the change in the strahl intensity (See also Borovsky (2020a) for a statistical study of the co-locations of strahl-intensity changes with strong current sheets.). Note in the bottom panel of **Figure 6** that as the strahl intensity decreases, the two calculated angles θ_{PS} indicate that the solar-wind magnetic field makes a transition from Parker-spiral aligned to not-Parker-spiral aligned.

Figure 7 is similar to **Figure 6**, where an increase in the strahl intensity occurs in the top panel of **Figure 7** at 2:54 UT on October 29 (Day 302) of 2005. That increase is marked by a vertical black dashed line. In the middle panel of **Figure 7** the increase in the strahl intensity is accompanied by an increase the proton temperature T_p (purple) and the proton specific entropy S_p (red) and by a decrease in the alpha-to-proton number-density ratio α/p (orange). The bottom panel of **Figure 7** indicates the presence of a strong current sheet at the location of the strahl change (the red $\Delta\theta$ curve) and the solar-wind magnetic field makes a transition from a non-Parker-spiral orientation to a more-Parker-spiral orientation.

Two causes of scattering for the electron strahl that have been well explored in the literature are Coulomb scattering (Scudder and Olbert, 1979; Lemons and Feldman, 1983; Boldyrev et al., 2020) and scattering by whistler waves (Gary et al., 1975; Saito and Gary, 2007; Viñas et al., 2010). The different mechanisms can cause scattering of the strahl at different electron energies. The rate of fast-electron angular scattering by Coulomb collisions S_{Coulomb} is proportional to the background number density n of the plasma (cf. eq. (6.4.10) of Krall and Trivelpiece (1973) or Sect.

3 of Tang et al., (2018)), written $S_{\text{Coulomb}} \propto n$. For strahl angular scattering by whistler turbulence with a fixed amplitude, modeling indicates that the scattering rate is approximately proportional to B^3/n times a weak power n/B^2 , resulting approximately in $S_{\text{whistler}} \propto B^2/n^{1/2}$ (cf. eq. (B4) of Steinacker and Miller (1992), eq. (8) of Pierrard et al., (2011), or Sect. 3 of Tang et al., (2018)). For angular scattering by kinetic-Alfven-wave turbulence, eq. (30) of Boldyrev and Horiates. (2019) gives $S_{\text{kineticAlfven}} \propto n$.

Using the 64-sec-resolution ACE plasma SWEPAM and magnetic-field MAG data for the year 2005, 528 strong changes in the intensity of the electron strahl at 1 AU were analyzed: 282 of those 528 strahl changes occurred when the solar-wind plasma was categorized as sector-reversal-region plasma and 246 of the strahl changes occurred in wind with $v_{\text{sw}} < 460$ km/s that was categorized as either ejecta or streamer-belt-origin plasma. This list of jumps collected in 2005 is by no means exhaustive. Only 528 jumps were collected owing to the restrictions 1) that the jumps must occur in sector-reversal-region plasma or in the slow wind surrounding sector-reversal-region plasma, 2) a jump must represent an increase or a decrease in the strahl intensity that is a change in the intensity of about 50% or greater in the timescale of 1 or two data points, 3) that there must be a clear persistence in the strahl intensity for a few minutes both before and after the jump, and 4) there must be strahl and plasma measurements free of nearby data dropouts. This latter restriction was the strongest because validated ACE SWEPAM proton-plasma measurements are typically absent when the solar-wind speed goes very low, as it tends to do in sector-reversal-region plasma. The statistical analysis of the 528 strahl-intensity changes from the year 2005 is summarized in **Table 1** and graphically represented in **Figure 8**.

For the strong changes in the intensity of the electron strahl, attention was paid to the sign of simultaneous changes in the magnetic-field strength B_{mag} , the proton number density n_p , the proton temperature T_p , the proton specific entropy $S_p = T_p/n_p^{2/3}$, the alpha-to-proton number-density ratio α/p , and the change in the angle θ_{PS} between the magnetic-field orientation and the Parker-spiral direction. A change in each of the parameters was only recorded 1) if the parameter exhibited a simultaneous shift (jump) in its magnitude and 2) if the shift change was larger than the fluctuation levels of that parameter prior to and after the change. A change in θ_{PS} was only recorded if the field direction strongly changed from an orientation that would definitely be categorized as Parker-spiral-oriented to an orientation that would definitely be categorized as not-Parker-spiral-oriented (a positive change) or if the direction strongly changed from definitely not-Parker-spiral-oriented to definitely Parker-spiral-oriented (a negative change) (These are typically angular changes by greater than 45°). For all 528 changes in the strahl intensity, the statistics of simultaneous changes in those other quantities are collected into **Table 1**. The first three data columns of **Table 1** contain the fraction of time that the change was in the same direction as the strahl-intensity change, (i.e. both simultaneously increasing or both simultaneously decreasing), the fraction of time that the changes were in the opposite directions, and the fraction of time that there was a change in the strahl intensity but

TABLE 1 | The statistical connection of strahl-intensity changes to changes in other plasma parameters in the year 2005.

Quantity	Set of strahl jumps	Change opposite to I_{272} (%)	No change observed (%)	Change same direction as I_{272} (%)	Fraction of time a change is seen (%)	Ratio same to opposite
S_p	All 528	10.6	42.0	47.4	58.0	4.47/1
	SRR plasma	11.0	40.4	48.6	59.6	4.42/1
	Other slow	10.2	43.9	45.9	56.1	4.52/1
n_p	All 528	31.3	57.0	11.7	43.0	1/2.66
	SRR plasma	34.8	53.6	11.7	46.6	1/2.97
	Other slow	27.2	61.0	11.8	39.0	1/2.30
T_p	All 528	13.4	43.6	43.0	56.4	3.20/1
	SRR plasma	12.1	46.5	41.5	53.6	3.44/1
	Other slow	15.0	40.2	44.7	59.7	2.97/1
B_{mag}	All 528	8.9	64.4	26.7	35.6	3.00/1
	SRR plasma	12.4	55.7	31.9	44.3	2.57/1
	Other slow	4.9	74.4	20.7	25.6	4.25/1
α/p	All 528	16.4	70.8	12.9	29.3	1/1.27
	SRR plasma	19.0	67.7	13.3	32.3	1/1.43
	Other slow	13.2	74.4	12.4	25.6	1/1.07
θ_{ps}	All 528	24.1	69.5	6.4	30.5	1/3.73
	SRR plasma	22.0	69.2	8.9	30.9	1/2.48
	Other slow	26.4	69.9	3.7	30.1	1/7.22

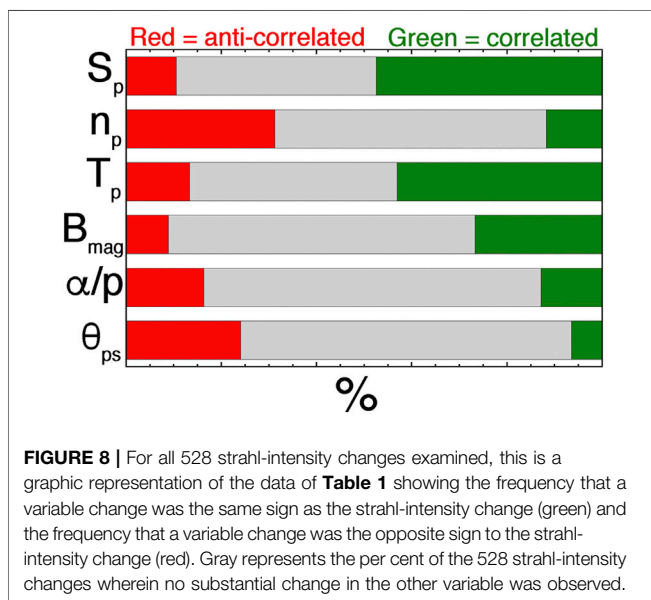


FIGURE 8 | For all 528 strahl-intensity changes examined, this is a graphic representation of the data of **Table 1** showing the frequency that a variable change was the same sign as the strahl-intensity change (green) and the frequency that a variable change was the opposite sign to the strahl-intensity change (red). Gray represents the per cent of the 528 strahl-intensity changes wherein no substantial change in the other variable was observed.

no change in the other quantity that was larger than the noise level in the measurements. Each set of three rows in **Table 1** represents the statistics for all of the 528 strahl changes, the statistics for the 282 strahl changes in sector-reversal-region plasma, and the statistics for the 246 strahl changes in other slow solar-wind types. Note for each variable that the statistical numbers in **Table 1** are similar for each of the three rows: the similarity in the statistics of the 282 sector-reversal-region plasma strahl changes and of the 246 other strahl changes indicates that the statistical results are robust since similar values are obtained for two independent sets of events. For “All 528” rows of **Table 1**, the first three columns are graphically represented in **Figure 8**,

with green corresponding to changes of the same sign (correlation), red corresponding to changes of the opposite sign (anti-correlation), and gray representing no clear changes observed. The second from the last column of **Table 1** is the fraction of strahl-change events that had observed changes in the other quantity of interest. In **Table 1** the strongest connections with strahl-intensity changes are for the variables S_p and T_p , with 58% and 56% of the strahl changes being accompanied by changes in these two variables, respectively. Note that only 35.6% of the strahl changes have B_{mag} changes accompanying them; further, since the B_{mag} measurements in the ACE 64-sec data set have very low noise, it is easier to find a B_{mag} change if it occurs than it is with the other plasma variables. Still only 35.6% of the strahl-intensity changes had B_{mag} changes: hence the connection of B_{mag} changes to strahl changes is considerably weaker than the connection of other plasma variables to strahl changes. Note also that changes in the angle θ_{ps} between the magnetic-field orientation and the Parker-spiral direction are only counted as nonzero if the angle change is very strong, (e.g. going between a very low angle to something greater than 45° or vice versa); hence, in reality the connection of strahl-intensity changes to the transition between Parker-spiral aligned and not Parker-spiral aligned is probably greater than the $\sim 31^\circ$ recorded in **Table 1**.

The final column of **Table 1** contains the ratio of the number of changes that were of the same sign as the strahl-intensity change to the number of changes that were of the opposite sign as the strahl-intensity change. Changes in the strahl-intensity were positively correlated with changes in S_p , T_p , and B_{mag} and changes in the strahl intensity were anti-correlated with changes in n_p , α/p , and θ_{ps} . The strongest connections to the strahl change were for S_p and T_p . For all of the 528 strahl changes, S_p changes that were of the same sign as the strahl-intensity changes were 4.47 times as likely to be found as S_p changes that were of the opposite sign as the strahl change. Hence, same-sign changes are

TABLE 2 | For all solar-wind data, the Pearson linear correlation coefficients between hourly averaged solar-wind parameters including the strahl intensity $I_{272} = \text{Log}_{10}(f_{272})$.

	I_{272}	Log (S_p)	Log (T_p)	Log (n_p)	v_{sw}	Log (B_{mag})	α/p	δB_{vec}	Log (C^{6+}/C^{4+})	Log (C^{6+}/C^{5+})	Log (O^{7+}/O^{6+})	Log (Fe/O)	θ_{PS} equatorial	θ_{PS} 3-D
I_{272}	1	0.22	0.33	0.11	0.16	0.63	0.28	0.34	0.09	0.04	0.10	0.08	-0.16	-0.15
Log (S_p)	0.22	1	0.91	-0.64	0.77	0.15	0.30	0.26	-0.40	-0.32	-0.55	-0.35	-0.13	-0.18
Log (T_p)	0.33	0.91	1	-0.26	0.70	0.31	0.30	0.46	-0.37	-0.32	-0.52	-0.34	-0.13	-0.15
Log (n_p)	0.11	-0.64	-0.26	1	-0.47	0.22	-0.16	0.25	0.25	0.16	0.31	0.17	0.07	0.12
v_{sw}	0.16	0.77	0.70	-0.47	1	0.20	0.27	0.30	-0.50	-0.50	-0.48	-0.33	-0.04	-0.07
Log (B_{mag})	0.63	0.15	0.31	0.22	0.20	1	0.32	0.51	0.12	0.05	0.19	0.13	-0.10	-0.05
α/p	0.28	0.30	0.30	-0.16	0.27	0.32	1	0.22	-0.09	-0.13	0.06	-0.02	-0.05	-0.06
δB_{vec}	0.34	0.26	0.46	0.25	0.30	0.51	0.22	1	-0.06	-0.08	-0.10	-0.05	-0.04	0.01
Log (C^{6+}/C^{4+})	0.09	-0.40	-0.37	0.25	-0.49	0.16	-0.09	-0.06	1	0.93	0.79	0.25	0.06	0.09
Log (C^{6+}/C^{5+})	0.04	-0.32	-0.32	0.16	-0.50	0.05	-0.13	-0.08	0.93	1	0.69	0.23	0.06	0.08
Log (O^{7+}/O^{6+})	0.10	-0.55	-0.52	0.31	-0.48	0.19	0.06	-0.10	0.79	0.69	1	0.42	0.11	0.148
Log (Fe/O)	0.08	-0.35	-0.34	0.17	-0.33	0.13	-0.02	-0.05	0.25	0.23	0.42	1	0.03	0.06
θ_{PS} equatorial	-0.16	-0.13	-0.13	0.07	-0.04	-0.10	-0.05	-0.04	0.06	0.06	0.11	0.03	1	0.86
θ_{PS} 3-D	-0.15	-0.18	-0.15	0.12	-0.07	-0.05	-0.06	0.01	0.09	0.08	0.15	0.06	0.86	1

greatly preferred. For T_p that ratio in **Table 1** is 3.20 to 1. B_{mag} changes were 3.0 times as likely to be of the same sign of the strahl-intensity changes than to be of the opposite sign, but B_{mag} changes were only observed for 35.6% of the strahl changes.

Overall, changes in the alpha-to-proton number-density ratio α/p are poorly connected to strahl-intensity changes, with only 29.3% of the strahl changes having clearly identified changes in α/p , and the number of changes of α/p that were of the same sign as the strahl changes was about equal to the number of α/p changes that were of the opposite sign.

For changes in the strahl intensity caused by changes in the amount of whistler-turbulence scattering of the strahl (with the strength of the scattering going approximately as $S_{whistler} \propto B^2/n^{1/2}$), one would expect the strahl intensity to increase when B_{mag} decreases and/or when n_p increases: however, **Table 1** indicates that the opposite tends to occur for both B_{mag} and n_p .

For changes in the strahl intensity caused by changes in the amount of Coulomb scattering or in the amount of kinetic-Alfven-wave turbulence scattering (with $S_{Coulomb} \propto n$ and with $S_{kineticAlfven} \propto n$), one would expect the strahl intensity to increase when the number density n_p decreases, which is seen in **Table 1** strahl-change association between the strahl intensity and n_p . However, n_p changes are only seen for 43.0% of the strahl-intensity changes and the changes with T_p and with S_p are stronger than the changes with n_p . **Table 1** yields weak support for strahl scattering by Coulomb collisions or by kinetic Alfven waves.

In the associations of **Table 1** there is modest support for the notion that transfers from Parker-spiral-oriented plasma to non-Parker-spiral-oriented plasma result in a decrease in the intensity of the strahl, and that transfers from non-Parker-spiral-oriented plasma to Parker-spiral-oriented plasma result in an increase in the intensity of the strahl.

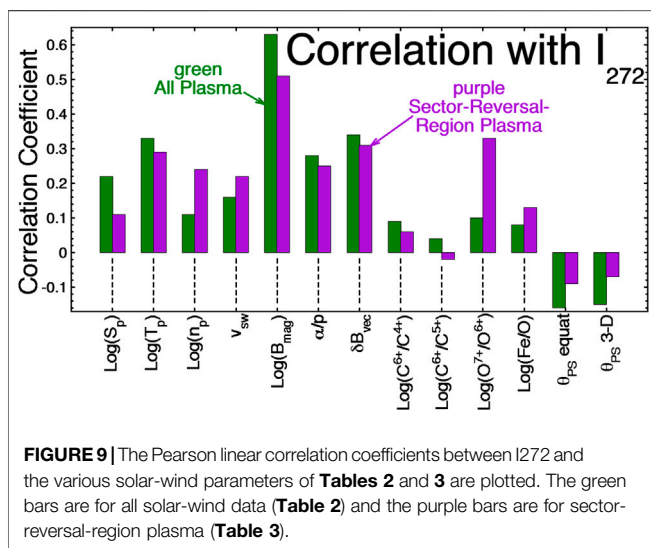
Note that the relations between changes in the strahl intensity at 1 AU and changes in the plasma properties at 1 AU are examined via **Table 1** and interpretations are made; however, the changes across these same strahl-intensity boundaries closer to

the Sun than 1 AU may differ in nature from the changes observed at 1 AU across the boundaries.

Further information about the strahl intensity is provided by **Tables 2** and **3**, which contain the Pearson linear correlation coefficients between the hourly averages of the logarithm of the strahl intensity $I_{272} = \text{Log}_{10}(f_{272})$ at Earth and hourly averages of various solar-wind parameters at Earth. The correlations of I_{272} with solar-wind parameters listed in **Tables 2** and **3** are also graphically represented in **Figure 9**. **Tables 2** and **3** also provide information about the intercorrelations among the solar-wind variables. Note that the logarithms of some variables are used in the correlations: for some variables (e.g. n_p , S_p , T_p , and B_{mag}) this keeps outlier values from strongly affecting the correlation coefficients and other variables are ratios (e.g. C^{6+}/C^{4+} , C^{6+}/C^{5+} , O^{7+}/O^{6+} , and Fe/O) and using the logarithm of the ratio gives more weight in the correlations to extremely small values of the ratio; in other words, the logarithms of these variables are closer to Gaussian distributed. **Table 2** pertains to all solar-wind data and **Table 3** pertains to times when the solar wind is categorized as sector-reversal-region plasma. The strahl-correlation information of **Tables 2** and **3** is related to, but not exactly the same as, the information in **Table 1**. The information of **Table 1** addresses the question: when the strahl-intensity changes, does a particular plasma quantity X make a change in the same direction? The information of **Tables 2** and **3** addresses the question: how well can the value of I_{272} be predicted if there is a knowledge of the value of the plasma quantity X? **Tables 2** and **3** also address the question: are large values of X related to large values of I_{272} and are small values of X related to small values of I_{272} ? **Tables 2** and **3** utilize hourly averaged values of the electron strahl from ACE SWEPAM, hourly averaged values of the solar-wind plasma and field parameters from OMNI2, and hourly averaged heavy-ion measurements from ACE SWICS (Gloeckler et al., 1998) (the "1.1" version of the SWICS data set). The strahl values in the years 1998–2013 are used. In **Tables 2** and **3** δB_{vec} is the rms

TABLE 3 | For sector-reversal-region plasma, the Pearson linear correlation coefficients between hourly averaged solar-wind parameters including the strahl intensity $I_{272} = \text{Log}_{10}(I_{272})$.

	I_{272}	Log (S_p)	Log (T_p)	Log (n_p)	v_{sw}	Log (B_{mag})	α/p	δB_{vec}	Log (C^{6+}/C^{4+})	Log (C^{6+}/C^{5+})	Log (O^{7+}/O^{6+})	Log (Fe/O)	θ_{PS} equatorial	θ_{PS} 3-D
I_{272}	1	0.11	0.29	0.24	0.22	0.51	0.25	0.31	0.06	-0.02	0.33	0.13	-0.09	-0.07
Log (S_p)	0.11	1	0.74	-0.35	0.31	0.06	0.16	0.12	0.13	0.22	-0.25	-0.02	0.00	-0.01
Log (T_p)	0.29	0.74	1	0.37	0.36	0.37	0.20	0.47	0.05	0.07	-0.07	-0.04	-0.01	0.01
Log (n_p)	0.24	-0.35	0.37	1	0.07	0.43	0.06	0.48	-0.12	-0.21	0.25	-0.01	-0.02	0.03
v_{sw}	0.22	0.31	0.36	0.07	1	0.18	0.29	0.21	-0.18	-0.28	0.21	-0.09	0.09	0.10
Log (B_{mag})	0.51	0.06	0.37	0.43	0.18	1	0.26	0.50	-0.06	-0.13	0.23	0.14	-0.07	-0.03
α/p	0.25	0.16	0.20	0.06	0.29	0.26	1	0.15	-0.25	-0.38	0.46	0.11	0.04	0.04
δB_{vec}	0.31	0.12	0.47	0.48	0.21	0.50	0.15	1	-0.05	-0.07	0.06	0.08	-0.02	0.05
Log (C^{6+}/C^{4+})	0.06	0.13	0.05	-0.12	-0.18	-0.06	-0.25	-0.05	1	0.89	0.24	-0.10	-0.06	-0.06
Log (C^{6+}/C^{5+})	-0.02	0.22	0.07	-0.21	-0.28	-0.13	-0.38	-0.07	0.89	1	0.01	-0.04	-0.05	-0.06
Log (O^{7+}/O^{6+})	0.33	-0.25	-0.07	0.25	0.21	0.23	0.46	0.06	0.24	0.01	1	0.14	0.00	0.01
Log (Fe/O)	0.13	-0.02	-0.04	-0.01	-0.09	0.14	0.11	0.08	-0.10	-0.04	0.14	1	-0.00	0.00
θ_{PS} equatorial	-0.09	0.00	-0.01	-0.02	0.09	-0.07	0.04	-0.02	-0.06	-0.05	0.00	-0.00	1	0.85
θ_{PS} 3-D	-0.07	-0.01	0.01	0.03	0.10	-0.03	0.04	0.05	-0.06	-0.06	0.01	0.00	0.85	1



amplitude of the vector magnetic-field fluctuations in each hour of data and $\delta B_{vec}/B_{mag}$ is the amplitude of the wobble angle (in radians) of the solar-wind magnetic-field vector during each hour. In **Tables 2** and **3** the angle θ_{PS} between the magnetic-field direction and the Parker-spiral direction is calculated two ways: 1) the direction of the equatorial projection of the magnetic field from the Parker-spiral direction and 2) the full 3-D direction of the field with respect to the Parker-spiral direction. The latter includes the B_z (or B_n) component of the field. For the sake of correlation coefficients it does not matter, but the logarithms are base-10 logarithms. The statistical noise in the correlation coefficients of **Tables 2** and **3** is very low. For N points correlated, the statistical noise level on the correlation coefficient is $2/(N+1)^{1/2}$ (Beyer, 1966; Bendat and Piersol, 1971). In **Table 2** there are $N = 127,130$ data points for I_{272} yielding a

statistical noise level of ± 0.006 for the correlation coefficients and in **Table 3** there are $N = 25,569$ data points for I_{272} yielding a statistical noise level of ± 0.013 for the correlation coefficients.

Between the all-solar-wind **Table 2** and the sector-reversal-region-plasma **Table 3** there are often substantial variations of the correlation coefficients between solar-wind variables. In the all-solar-wind correlations of **Table 2**, many of the correlations and anti-correlations are set up 1) by large-scale compressions and rarefactions of the solar-wind plasma owing to large variations in the solar-wind speed and 2) by solar-rotation-driven sequential switching between plasma types that have systematic differences in their parameters (cf. Borovsky, 2018). In the sector-reversal-region plasma correlations of **Table 3**, neither of those two mechanisms operate since 1) the range of sector-reversal-region-plasma velocities is quite limited and 2) there is only one type of solar-wind plasma. In general, since the data used in **Table 3** is a subset of the data used in **Table 2**, and since that subset is chosen by restricting the range of some of the solar-wind parameters, the correlation coefficients in **Table 3** are expected to be of a lower magnitude than the coefficients in **Table 2**. Noticeable correlations with I_{272} that are actually higher in the sector-reversal-region-plasma **Table 3** than in the all-wind **Table 2** are the correlations of I_{272} with Log (n_p), with v_{sw} , and with Log (O^{7+}/O^{6+}) (see also **Figure 9**).

In **Table 3** the strongest correlations of I_{272} are with Log (B_{mag}). If the field-aligned flux of the electron strahl is conserved, then a positive correlation between I_{272} and B_{mag} is expected, (e.g. in **Tables 1–3** and **Figure 9**); this is very clearly seen in CIR compressions and trailing-edge rarefactions where the magnetic-field lines are squeezed together or expanded apart and the strahl-intensity pattern tracks the magnetic-field-strength pattern (Crooker et al., 2010; Borovsky, 2016). The next strongest I_{272} correlations in **Table 3** are with Log (O^{7+}/O^{6+}), δB_{vec} , and Log (T_p) (with δB_{vec} being strongly correlated with B_{mag}). Comparing

the I_{272} correlations of **Table 3** with the strahl-change findings of **Table 1**, the correlations of **Table 3** support the positive correlations of strahl-intensity changes with changes in S_p , T_p , and B_{mag} and the correlations of **Table 3** support the anti-correlations of strahl-intensity changes with changes in θ_{PS} . The positive correlations of I_{272} with n_p and α/p in **Table 3** are counter to **Table 1** findings of anti-correlations between changes in the strahl intensity and changes in n_p and α/p . Of course, in using the correlations of **Table 3** as support or not support of the strahl-change trends of **Table 1**, it must be realized that the factors that drive the large-scale correlation with strahl intensity (**Table 3**) may not be the same factors that drive the sudden ~50% strahl-intensity changes of **Table 1**.

DISCUSSION: INTERPRETATION OF STRAHL-INTENSITY CHANGES, ASSESSING THE SUN-EARTH CONNECTION, AND THE FUTURE

Being aware that different mechanisms can act on different energy electrons in the strahl, examining 272 eV strahl-intensity changes in sector-reversal-region plasma and other slow solar wind (**Table 1**) found that increases or decreases of the strahl intensity are positively correlated with S_p , T_p , and B_{mag} increases or decreases and that strahl-intensity increases or decreases are anti-correlated with n_p , θ_{PS} , and α/p increases or decreases. Relevant to the B_{mag} and α/p anti-correlations, note that 1) most (64.4%) strahl-intensity changes do not show B_{mag} changes and 2) the association of α/p changes with strahl changes is weak.

The results of the 272 eV strahl-change analysis are inconsistent with a constant-amplitude model for whistler-turbulence scattering of the strahl as the reason for the strahl-intensity changes; for whistler scattering the changes in the strahl intensity should be correlated with n_p changes and anti-correlated with B_{mag} changes and the opposite correlations are observed. The 272 eV strahl-change analysis weakly supports Coulomb scattering and/or kinetic-Alfven-wave scattering as the cause of strahl-intensity changes; the support is only weak because the expected strahl-intensity-change anti-correlation with n_p is not the strongest association with strahl changes (Further, **Table 3** solar-wind correlations show that the strahl intensity positively correlates with n_p). The strongest connection of strahl-intensity changes is with changes in T_p and S_p , which are not involved in the Coulomb-scattering, whistler-scattering, or kinetic-Alfven-wave scattering scenarios.

The strongest associations with strahl-intensity changes are the positive correlations with changes in S_p and T_p (**Table 1**). The factors that govern the values of S_p and T_p in the solar wind are not well understood. The value of the proton specific entropy S_p of the solar wind at 1 AU is a strong indicator of the plasma type (cf. Figure 3 of Xu and Borovsky (2015)). Excluding ejecta plasma, the proton temperature T_p of the solar wind at 1 AU is strongly associated with v_{sw} (cf. Figure 1 of Lopez and Freeman (1986), Figure 12 of Borovsky and Steinberg (2006), Figures. 4 and 5 of

Elliott et al., (2012)). The proton specific entropy S_p is also strongly positively correlated with v_{sw} (cf. **Tables 2** and **3**).

In the slower solar wind (such as sector-reversal-region plasma) it is well known that the observed solar-wind velocity v_{sw} systematically increases with distance from the Sun beyond 0.3 AU (Schwenn et al., 1981; Arya and Freeman, 1991): this could be the result of a hot-electron-driven interplanetary ambipolar electric potential accelerating the solar-wind protons away from the Sun (Jockers, 1970; Lemaire, 2010; Pierrard, 2012; Borovsky and Gary, 2014). The strahl-change (**Table 1**) and strahl-correlation (**Table 3**) data indicates that weaker sector-reversal-region-plasma strahls are related to weaker proton temperatures and weaker proton specific entropies and the correlation data indicates that weaker strahls are associated with slower solar wind at 1 AU. These correlations could be consistent with weaker electron-driven interplanetary electric field owing to poor magnetic connection to the corona or to connections that produce poor strahl. Note however that the correlation coefficients in **Table 3** are weak, indicating that strahl intensity is not the dominant driver of the proton values.

In the all-solar-wind data set (**Table 2**) S_p is strongly anti-correlated with the heavy-ion charge state ratios C^{6+}/C^{4+} , C^{6+}/C^{5+} , and O^{7+}/O^{6+} , but in sector-reversal-region plasma (**Table 3**) these correlations become complicated with S_p being anti-correlated with C^{6+}/C^{4+} and C^{6+}/C^{5+} and positively correlated with O^{7+}/O^{6+} . The oxygen-charge-state relation to the carbon-charge states differs in sector-reversal-region plasma (and ejecta) from its relation in coronal-hole-origin plasma and streamer-belt-origin plasma (cf. Figures. 10 and 12 of Xu and Borovsky (2015) and Figure 1 of Zhao et al., (2016)); Xu and Borovsky (2015) speculated that this carbon-oxygen charge-state relation is an indicator of impulsive vs. steady emission of plasma from the corona, with sector-reversal-region plasma being impulsive at times.

The strahl-change analysis also finds an anti-correlation between changes in the strahl intensity and changes in the angle θ_{PS} of the magnetic field from the Parker-spiral direction: this is consistent with stronger strahl in Parker-spiral plasma (continuously emitted with open magnetic flux from the corona) vs. non-Parker-spiral plasma (impulsively emitted, perhaps with magnetic disconnections). There may, however, be magnetic-pathlength differences between Parker-spiral fields and non-Parker-spiral fields that might also be playing a role in the 1-AU strahl intensity.

Examining the sudden changes in the intensity of the electron strahl at 1 AU accompanied by sudden changes in the magnetic-field direction, Gosling et al., (2004A,B) speculated that abrupt changes in the strahl intensity are the manifestations of abrupt changes in the mapping of the solar-wind magnetic field back to the corona. In the strahl-change statistics of **Table 1**, strong changes in the field direction from Parker-spiral oriented to non-Parker-spiral oriented could account for ~25% of the strahl changes. This change in connection to the corona is also supported by the plasma-property changes found to accompany strahl-intensity changes (**Table 1**) (However in **Table 1** the weakest connection of strahl change is with α/p , which should change with magnetic connection to the corona.) Further, this change-in-magnetic-

connection picture is supported by the above-the-corona MHD simulations of Burkholder et al., (2019) where current sheets in the plasma represent topological changes in the magnetic mapping back to the photosphere.

Sector-reversal-region plasma at 1 AU is characterized by a wide range of low strahl intensities and by sudden changes in the strahl intensity. Analysis of the strahl-intensity changes at 1 AU imply that the changes in the strahl intensity are caused by changes in the magnetic connection to the corona. When the strahl-intensities change to low values a question is: Which low values represent a lack of magnetic connection to the Sun and which low values are caused by something else? A related question is: Why is the strahl intensity so low if it is still magnetically connected to the corona?

Analysis of strahl intensity during impulsive SEE events was used to test the idea that strahl presence or absence could be used to assess the magnetic connection to the Sun. This test was based on the assumption that SEE events at Earth can only occur when the Earth is well connected magnetically to the Sun. The SEE test was not helpful in making the assessment: SEE event occur during solar maximum and the analysis found that the strahl is almost always strong during solar maximum.

To assess the quality of the magnetic connection between the near-Earth solar wind and the Sun, three tools have been explored: 1) using the strahl intensity, 2) using the orientation θ_{PS} of the solar-wind magnetic field with respect to the Parker-spiral direction, and 3) using the type of solar-wind plasma. Using the strahl intensity is the most promising, although questions remain when the strahl intensity at 1 AU is low: 1) is the magnetic field disconnected from the Sun, 2) is the magnetic field connected to a region of the corona that is producing poor strahl, or 3) has the strahl been destroyed between the Sun and 1 AU? Using the magnetic-field orientation θ_{PS} , along with an observation of the strahl intensity, provides more indication of whether or not the magnetic field is disconnected from the Sun. Using the plasma categorization “sector-reversal-region plasma” (with the categorization made using only proton measurements and the magnetic-field strength (Xu and Borovsky, 2015)) gives an indication of generally weak and intermittent strahl and the probability of an in-general poor or intermittent magnetic connection to the Sun.

Five suggestions are given for future research, mostly focused on the changes in strahl-intensity. 1) An examination is needed of the connection between strahl-intensity changes and the heavy-ion charge-state ratios of the solar-wind plasma. Such information is important in determining the nature of the change in the magnetic connection into the corona that may be occurring when there is a change in the strahl intensity and a change in the magnetic-field orientation. Such an examination has been recently enabled by the heavy-ion measurements onboard Solar Orbiter with ≤ 30 -s time resolution (Owen et al., 2020), measurements that are an order of magnitude faster than on previous solar-wind missions. 2) Examination of strahl changes on spacecraft closer to the Sun is important for a

better determination of the interpretation of strahl-intensity changes. An analysis with Parker Solar Probe in particular will be helpful, especially after a substantial data base is collected. 3) Often at 1 AU a sudden change is seen in the intensity of the anti-strahl: this change can be simultaneous with a change in the strahl or it can occur without a change in the strahl (An example of this can be seen at 3.37 UT in the blue curve the top panel of **Figure 7**.) A statistical examination of anti-strahl intensity changes might provide insight into the physics of strahl changes. It is also a method of exploring the magnetic topology beyond 1 AU. 4) The connection of strahl-intensity changes to whistler scattering made in the present study are based on a model of whistler scattering in the heliosphere that does not account for factors that could control the whistler-turbulence amplitude in the solar wind. Improvements in the prediction of the solar-wind parameters that control the amplitude of whistler turbulence in the solar wind and the resulting electron scattering are needed for an improved assessment of the role of whistlers in the observed strahl-intensity changes. 5) Another possible reason why a strahl may not be detected at 1 AU is because of plasma-wave instabilities that may have disrupted the strahl, (e.g. Gary and Saito, 2007; Kuzichev et al., 2019; Lopez et al., 2019; Vasko et al., 2019; Versharen et al., 2019; Jeong et al., 2020; Micera et al., 2020). Parameterization of instability thresholds is needed and then a matching of strahl-change locations with plasma-parameter changes is needed to test the instability possibility.

DATA AVAILABILITY STATEMENT

Publicly available datasets were analyzed in this study. This data can be found here: <http://www.srl.caltech.edu/ace/ASC/>.

AUTHOR CONTRIBUTIONS

The author confirms being the sole contributor of this work and has approved it for publication.

FUNDING

This work was supported by the NSF SHINE program via grant AGS-1723416, by the NASA Heliophysics Guest Investigator Program via award NNX17AB71G, by the NSF GEM Program via grant AGS-2027569, and by the NASA Heliophysics LWS program via award NNX16AB75G.

ACKNOWLEDGMENTS

The author thanks Stas Boldyrev, Ed Cliver, Larry Kepko, Ruth Skoug, John Steinberg, Nikki Vial for help and helpful conversations.

REFERENCES

- Amaya, J., Dupus, R., Innocenti, M. E., and Lapenta, G. (2020). Visualizing and interpreting unsupervised solar wind classifications. *Front. Astron. Space Sci.* 7, 553207. doi:10.3389/fspas.2020.553207
- Arya, S., and Freeman, J. W. (1991). Estimates of solar wind velocity gradients between 0.3 and 1 AU based on velocity probability distributions from Helios 1 at perihelion and aphelion. *J. Geophys. Res.* 96, 14183. doi:10.1029/91ja01135
- Bemporad, A., Sterling, A. C., Moore, R. L., and Poletto, G. (2005). A new variety of coronal mass ejection: streamer puffs from compact ejective flares. *Astrophys. J.* 635, L189. doi:10.1086/499625
- Bendat, J. S., and Piersol, A. G. (1971). *Random data: analysis and measurement procedures*. New York, NY, United States: John Wiley, Sect. 4.8.1.
- Bercic, L., Larson, D., Whittlesey, P., Maksimovic, M., Badman, S. T., Landi, S., et al. (2020). Coronal electron temperature inferred from the strahl electrons in the inner heliosphere: Parker Solar Probe and Helios observations. *Astrophys. J.* 892, 88. doi:10.3847/1538-4357/ab7b7a
- Beyer, W. H. (1966). *Handbook of Tables for Probability and statistics. Sect. IX*. Cleveland, OH, United States: Chemical Rubber Company.
- Bloch, T., Watt, C., Owens, M., McInnes, L., and Macneil, A. R. (2020). Data-driven classification of coronal hole and streamer belt solar wind. *Solar Phys.* 295, 41. doi:10.1007/s11207-020-01609-z
- Boldyrev, S., Forest, C., and Egedal, J. (2020). Electron temperature of the solar wind. *Proc. Natl. Acad. Sci. United States* 117, 9232. doi:10.1073/pnas.1917905117
- Boldyrev, S., and Horaites, K. (2019). Kinetic theory of the electron strahl in the solar wind. *MNRAS* 489, 3412. doi:10.1093/mnras/stz2378
- Borovsky, J. E. (2010). On the variations of the solar wind magnetic field about the Parker spiral direction. *J. Geophys. Res.* 115, A09101. doi:10.1029/2009ja015040
- Borovsky, J. E. (2016). The plasma structure of coronal hole solar wind: origins and evolution. *J. Geophys. Res.* 121, 5055. doi:10.1002/2016ja022686
- Borovsky, J. E. (2017). Time-integral correlations of multiple variables with the relativistic-electron flux at geosynchronous orbit: the strong roles of the substorm-injected electrons and the ion plasma sheet. *J. Geophys. Res.* 122, 11961. doi:10.1002/2017ja024476
- Borovsky, J. E. (2018). On the origin of the intercorrelations between solar-wind variables. *J. Geophys. Res.* 123, 20. doi:10.1002/2017ja024650
- Borovsky, J. E. (2020a). The magnetic structure of the solar wind: ionic composition and the electron strahl. *Geophys. Res. Lett.* 47, e2019GL084586. doi:10.1029/2019gl084586
- Borovsky, J. E. (2020b). Plasma and magnetic-field structure of the solar wind at inertial-range scale sizes discerned from statistical examinations of the time-series measurements. *Front. Astron. Space Sci.* 7, 20. doi:10.3389/fspas.2020.00020
- Borovsky, J. E., and Gary, S. P. (2014). How important are the alpha-proton relative drift and the electron heat flux for the proton heating of the solar wind in the inner heliosphere?. *J. Geophys. Res.* 119, 5210. doi:10.1002/2014ja019758
- Borovsky, J. E., and Steinberg, J. T. (2006). The freestream turbulence effect in solar-wind/magnetosphere coupling: analysis through the solar cycle and for various types of solar wind. *Geophys. Monog. Ser.* 167, 59. doi:10.1029/167gm07
- Bruno, R., and Bavassano, B. (1997). On the winding of the IMF spiral for slow and fast wind within the inner heliosphere. *Geophys. Res. Lett.* 24, 2267. doi:10.1029/97gl02183
- Burkholder, B. L., Otto, A., Delamere, P. A., and Borovsky, J. E. (2019). Magnetic connectivity in the corona as a source of structure in the solar wind. *J. Geophys. Res.* 124, 32. doi:10.1029/2018ja026132
- Burlaga, L. F., and Ness, N. F. (1997). Global patterns of heliospheric magnetic field polarities and elevation angles: 1990 through 1995. *J. Geophys. Res.* 102, 19731. doi:10.1029/97ja01568
- Camporeale, E., Care, A., and Borovsky, J. E. (2017). Classification of solar wind with machine learning. *J. Geophys. Res.* 122, 10910. doi:10.1002/2017ja024383
- Chollet, E. E., and Giacalone, J. (2011). Evidence of confinement of solar-energetic particles to interplanetary magnetic field lines. *Astrophys. J.* 728, 64. doi:10.1088/0004-637x/728/1/64
- Chollet, E., Skoug, R., Steinberg, J., Crooker, N., and Giacalone, J. (2010). Reconnection and disconnection: observations of suprathermal electron heat flux dropouts. *AIP Conf. Proc.* 1216, 600. doi:10.1063/1.3395937
- Cliver, E. W., and Ling, A. G. (2007). Electrons and protons in solar energetic particle events. *Astrophys. J.* 658, 1349. doi:10.1086/511737
- Crooker, N. U., Appleton, E. M., Schwadron, N. A., and Owens, M. J. (2010). Suprathermal electron flux peaks at stream interfaces: Signature of solar wind dynamics or tracer for open magnetic flux transport on the Sun?. *J. Geophys. Res.* 115, A11101. doi:10.1029/2008GM000822
- Crooker, N. U., Gosling, J. T., and Kahler, S. W. (2002). Reducing heliospheric magnetic flux from coronal mass ejections without disconnection. *J. Geophys. Res.* 107, 1028. doi:10.1029/2001ja000236
- Crooker, N. U., Huang, C.-L., Lamassa, S. M., Larson, D. E., Kahler, S. W., and Spence, H. E. (2004). Heliospheric plasma sheets. *J. Geophys. Res.* 109, A03107. doi:10.1029/2003ja010170
- Crooker, N. U., and Owens, M. J. (2012). Interchange reconnection: remote sensing of solar signature and role in heliospheric magnetic flux budget. *Space Sci. Rev.* 172, 201. doi:10.1007/s11214-011-9748-1
- Crooker, N. U., and Pagel, C. (2008). Residual strahls in solar wind electron dropouts: signatures of magnetic connection to the Sun, disconnection, or interchange reconnection? *J. Geophys. Res.* 113, A02106. doi:10.1029/2007ja012421
- Elliott, H. A., Henney, C. J., McComas, D. J., Smith, C. W., and Vasquez, B. J. (2012). Temporal and radial variation of the solar wind temperature-speed relationship. *J. Geophys. Res.* 117, A09102. doi:10.1029/2011ja017125
- Feldman, W. C., Asbridge, J. R., Bame, S. J., Gary, S. P., Montgomery, M. D., and Zink, S. M. (1976). Evidence for the regulation of solar wind heat flux at 1 AU. *J. Geophys. Res.* 81, 5207. doi:10.1029/ja081i028p05207
- Fisk, L. A. (2001). On the global structure of the heliospheric magnetic field. *J. Geophys. Res.* 106, 15849. doi:10.1029/2000ja000117
- Forsyth, R. J., Balogh, A., Smith, E. J., Erdős, G., and McComas, D. J. (1996). The underlying Parker spiral structure in the Ulysses magnetic field observations, 1990-1994. *J. Geophys. Res.* 101, 395. doi:10.1029/95ja02977
- Foullon, C., Lavraud, B., Luhmann, J. G., Farrugia, C. J., Retino, A., Simunac, K. D. C., et al. (2011). Plasmoid releases in the heliospheric current sheet and associated coronal hole boundary layer evolution. *Astrophys. J.* 737, 16. doi:10.1088/0004-637x/737/1/16
- Gary, S. P., Feldman, W. C., Forslund, D. W., and Montgomery, M. D. (1975). Electron heat flux instabilities in the solar wind. *Geophys. Res. Lett.* 2, 79-82. doi:10.1029/gl002i003p00079
- Gary, S. P., and Saito, S. (2007). Broadening of solar wind strahl pitch-angles by the electron/electron instability: particle-in-cell simulations. *Geophys. Res. Lett.* 34, L14111. doi:10.1029/2007gl030039
- Georgieva, K., Kirov, B., Javaraiah, J., and Krasteva, R. (2005). Solar rotation and solar wind-magnetosphere coupling. *Planet. Space Sci.* 53, 197. doi:10.1016/j.pss.2004.09.045
- Gloeckler, G., Cain, J., Ipavich, F. M., Tums, E. O., Bedini, P., Fisk, L. A., et al. (1998). Investigation of the composition of solar and interstellar matter using solar wind and pickup ion measurements with SWICS and SWIMS on the ACE spacecraft. *Space Sci. Rev.* 86, 497. doi:10.1007/978-94-011-4762-0_18
- Gosling, J. T., de Koning, C. A., Skoug, R. M., Steinberg, J. T., and McComas, D. J. (2004a). Dispersionless modulations in low-energy solar electron bursts and discontinuous changes in the solar wind electron strahl. *J. Geophys. Res.* 109, A05102. doi:10.1029/2003ja010338
- Gosling, J. T., Skoug, R. M., McComas, D. J., and Mazur, J. E. (2004b). Correlated dispersionless structure in suprathermal electrons and solar energetic ions in the solar wind. *Astrophys. J.* 614, 412. doi:10.1086/423368
- Gosling, J. T., Skoug, R. M., McComas, D. J., and Smith, C. W. (2005). Magnetic disconnection from the Sun: observations of a reconnection exhaust in the solar wind at the heliospheric current sheet. *Geophys. Res. Lett.* 32, L05105. doi:10.1029/2005gl022406
- Gosling, J. T., and Skoug, R. M. (2002). On the origin of radial magnetic fields in the heliosphere. *J. Geophys. Res.* 107, 1327. doi:10.1029/2002ja009434
- Hammond, C. M., Feldman, W. C., McComas, D. J., Phillips, J. L., and Forsyth, R. J. (1996). Variation of electron-strahl width in the high-speed solar wind: Ulysses observations. *Aston. Astrophys.* 316, 350-354.
- Heidrich-Meisner, V., Berger, L., and Wimmer-Schweingruber, R. F. (2020). Proton-proton collisional age to order solar wind types. *Aston. Astrophys.* 636, A103. doi:10.1051/0004-6361/201937378
- Jeong, S.-Y., Verscharen, D., Wicks, R. T., and Fazakerley, A. N. (2020). A quasi-linear diffusion model for resonant wave-particle instability in homogeneous plasma. *Astrophys. J.* 902, 128. doi:10.3847/1538-4357/abb099

- Jockers, K. (1970). Solar wind models based on exospheric theory. *Astron. Astrophys.* 6, 219.
- Kallenrode, M.-B., and Švestka, Z. (1994). The participation of nuclei in type-III-related electron streams. *Sol. Phys.* 155, 121. doi:10.1007/bf00670735
- Kepko, L., and Spence, H. E. (2003). Observations of discrete, global magnetospheric oscillations directly driven by solar wind density variations. *J. Geophys. Res.* 108, 1257. doi:10.1029/2002ja009676
- Kepko, L., Viall, N. M., Antiochos, S. K., Lepri, S. T., Kasper, J. C., and Weberg, M. (2016). Implications of L1 observations for slow solar wind formation by solar reconnection. *Geophys. Res. Lett.* 43, 4089. doi:10.1002/2016gl068607
- Kepko, L., and Viall, N. M. (2019). The source, significance, and magnetospheric impact of periodic density structures within stream interaction regions. *J. Geophys. Res.* 124, 2019JA026962. doi:10.1029/2019ja026962
- King, J. H., and Papitashvili, N. E. (2005). Solar wind spatial scales in and comparisons of hourly Wind and ACE plasma and magnetic field data. *J. Geophys. Res.* 110, 2104. doi:10.1029/2004ja010649
- Krall, N. A., and Trivelpiece, A. W. (1973). *Principles of plasma physics*. New York, NY, United States: McGraw-Hill.
- Kuzichev, I. V., Vasko, I. Y., Soto-Chavez, A. R., Tong, Y., Artemyev, A. V., Bale, S. D., et al. (2019). Nonlinear evolution of the whistler heat flux instability. *Astrophys. J.* 882, 81. doi:10.3847/1538-4357/ab3290
- Lavraud, B., Fargette, N., Reville, V., Szabo, A., Huang, J., Ruillard, A. P., et al. (2020). The heliospheric current sheet and plasma sheet during Parker Solar Probe's first orbit. *Astrophys. J. Lett.* 894, L19. doi:10.3847/2041-8213/ab8d2d
- Lavraud, B., Gosling, J. T., Rouillard, A. P., Fedorov, A., Opitz, A., Sauvaud, J.-A., et al. (2009). Observations of a complex solar wind reconnection exhaust from spacecraft separated by over 1800 R_E . *Sol. Phys.* 256, 379. doi:10.1007/s11207-009-9341-x
- Lemaire, J. (2010). Half a century of kinetic solar wind models. *AIP Conf. Proc.* 1216, 8. doi:10.1063/1.3395971
- Lemons, D. S., and Feldman, W. C. (1983). Collisional modification to the exospheric theory of solar wind halo electron pitch angle distributions. *J. Geophys. Res.* 88, 6881. doi:10.1029/ja088ia09p06881
- Li, C., Sun, L. P., Wang, X. Y., and Dai, Y. (2013). Coronal magnetic topology and the production of solar impulsive energetic electrons. *Astron. Astrophys.* 556, L2. doi:10.1051/0004-6361/201322072
- Li, H., Wang, C., Tu, C., and Xu, F. (2020). Machine learning approach for solar wind categorization. *Earth Space Sci.* 7, e2019EA000997. doi:10.1029/2019ea000997
- Lin, R. P., and Kahler, S. W. (1992). Interplanetary magnetic field connection to the Sun during electron heat flux dropouts in the solar wind. *J. Geophys. Res.* 97, 8203. doi:10.1029/92ja00230
- Lockwood, M. (2013). Reconstruction and prediction of variations in the open solar magnetic flux and interplanetary conditions. *Living Rev. Solar Phys.* 10, 4. doi:10.12942/lrsp-2013-4
- Lopez, R. A., Shaaban, S. M., Lazar, M., Poedts, S., Yoon, P. H., Micera, A., et al. (2019). Particle-in-cell simulations of the whistler heat-flux instability in solar wind conditions. *Astrophys. J. Lett.* 882, L8.
- Lopez, R. E., and Freeman, J. W. (1986). Solar wind proton temperature-velocity relationship. *J. Geophys. Res.* 91, 1701. doi:10.1029/ja091ia02p01701
- Louarn, P., Diéval, C., Génot, V., Lavraud, B., Opitz, A., Fedorov, A., et al. (2009). On the temporal variability of the "strahl" and its relationship with solar wind characteristics: STEREO SWEA observations. *Sol. Phys.* 259, 311–321. doi:10.1007/s11207-009-9402-1
- Maksimovic, M., Zouganelis, I., Chaufray, J.-Y., Issautier, K., Scime, E. E., Littleton, J. E., et al. (2005). Radial evolution of the electron distribution functions in the fast solar wind between 0.3 and 1.5 AU. *J. Geophys. Res.* 110, A09104. doi:10.1029/2005ja011119
- Mazur, J. E., Mason, G. M., Dwyer, J. R., Giacalone, J., Jokipii, J. R., and Stone, E. C. (2000). Interplanetary magnetic field line mixing deduced from impulsive solar flare particles. *Astrophys. J.* 532, L79. doi:10.1086/312561
- McComas, D. J., Bame, S. J., Barker, P., Feldman, W. C., Phillips, J. L., Riley, P., et al. (1998). Solar wind electron proton alpha monitor (SWEPAM) for the advanced composition explorer. *Space Sci. Rev.* 86, 563. doi:10.1007/978-94-011-4762-0_20
- McComas, D. J., Gosling, J. T., Phillips, J. L., Bame, S. J., Luhmann, J. G., and Smith, E. J. (1989). Electron heat flux dropouts in the solar wind: evidence for interplanetary magnetic field reconnection?. *J. Geophys. Res.* 94, 6907. doi:10.1029/ja094ia06p06907
- Micera, A., Zhukov, A. N., López, R. A., Innocenti, M. E., Lazar, M., Boella, E., et al. (2020). Particle-in-cell simulation of whistler heat-flux instabilities in the solar wind: heat-flux regulation and electron halo formation. *Astrophys. J. Lett.* 903, L23. doi:10.3847/2041-8213/abc0e8
- Murphy, N., Smith, E. J., and Schwadron, N. A. (2002). Strongly underwound magnetic fields in co-rotating rarefaction regions: observations and implications. *Geophys. Res. Lett.* 29, 2066. doi:10.1029/2002gl015164
- Ness, N. F., and Wilcox, J. M. (1966). Extension of the photospheric magnetic field into interplanetary space. *Astrophys. J.* 143, 23. doi:10.1086/148473
- Neugebauer, M., Reisenfeld, D., and Richardson, I. G. (2016). Comparison of algorithms for determination of solar wind regimes. *J. Geophys. Res.* 121, 8215. doi:10.1002/2016ja023142
- Neugebauer, M., Steinberg, J. T., Tokar, R. L., Barraclough, B. L., Dors, E. E., Wiens, R. C., et al. (2003). Genesis on-board determination of the solar wind flow regime. *Space Sci. Rev.* 105, 661. doi:10.1023/a:1024478129261
- Owen, C. J., Bruno, R., Livi, S., Louarn, P., and Al Janabi, K. (2020). The solar orbiter solar wind analyzer (SWA) suite. *Astron. Astrophys.* 642, A16. doi:10.1051/0004-6361/201937259
- Pagel, C., Crooker, N. U., and Larson, D. E. (2005a). Assessing electron heat flux dropouts as signatures of magnetic field line disconnection from the sun. *Geophys. Res. Lett.* 32, L14105. doi:10.1029/2005gl023043
- Pagel, C., Crooker, N. U., Larson, D. E., Kahler, S. W., and Owen, M. J. (2005b). Understanding electron heat flux signatures in the solar wind. *J. Geophys. Res.* 110, A01103. doi:10.1029/2004ja010767
- Parker, E. N. (1958). Dynamics of the interplanetary gas and magnetic fields. *Astrophys. J.* 128, 664. doi:10.1086/146579
- Pierrard, V., Lazar, M., and Schlickeiser, R. (2011). Evolution of the electron distribution function in the whistler wave turbulence of the solar wind. *Sol. Phys.* 269, 421. doi:10.1007/s11207-010-9700-7
- Pierrard, V. (2012). Solar wind electron transport: interplanetary electric field and heat conduction. *Space Sci. Rev.* 172, 315. doi:10.1007/s11214-011-9743-6
- Pilipp, W. G., Miggenrieder, H., Montgomery, M. D., Mühlhäuser, K.-H., Rosenbauer, H., and Schwenn, R. (1987). Characteristics of electron velocity distribution functions in the solar wind derived from the Helios Plasma experiment. *J. Geophys. Res.* 92, 1075. doi:10.1029/ja092ia02p01075
- Reames, D. V. (1999). Particle acceleration at the Sun and in the heliosphere. *Space Sci. Rev.* 90, 413. doi:10.1023/a:1005105831781
- Reisenfeld, D. B., Steinberg, J. T., Barraclough, B. L., Dors, E. E., Weins, R. C., Neugebauer, M., et al. (2003). Comparison of the Genesis solar wind regime algorithm results with solar wind composition observed by ACE. *AIP Conf. Proc.* 679, 632. doi:10.1063/1.1618674
- Riley, P., and Gosling, J. T. (2007). On the origin of near-radial magnetic fields in the heliosphere: numerical simulations. *J. Geophys. Res.* 112, A06115. doi:10.1029/2006ja012210
- Rouillard, A. P., Davies, J. A., Lavraud, B., Forsyth, R. J., Savani, N. P., Bewsher, D., et al. (2010). Intermittent release of transients in the slow solar wind: 1. Remote sensing observations. *J. Geophys. Res.* 115, A04103. doi:10.1029/2009ja014471
- Rouillard, A. P., Kouloumvakos, A., Vourlidis, A., Kasper, J., Bale, S., Raouafi, N.-E., et al. (2020). Relating streamer flows to density and magnetic structures at the parker solar robe. *Astrophys. J. Suppl. Ser.* 246, 37. doi:10.3847/1538-4365/ab579a
- Saito, S., and Gary, S. P. (2007). All whistlers are not created equally: scattering of strahl electrons in the solar wind via particle-in-cell simulations. *Geophys. Res. Lett.* 34, L01102. doi:10.1029/2006gl028173
- Sanchez-Diaz, E., Rouillard, A. P., Lavraud, B., Kilpua, E., and Davies, J. A. (2019). *In Situ* measurements of the variable slow solar wind near sector boundaries. *Astrophys. J.* 882, 51. doi:10.3847/1538-4357/ab341c
- Schwenn, R., Mühlhäuser, K.-H., Marsch, E., and Rosenbauer, H. (1981). Two states of the solar wind at the time of solar activity minimum II. Radial gradients of plasma parameters in fast and slow streams. *Solar wind four, MPAE-W-100-81-31*. Lindau, Germany: Max Planck Institut für Aeronomie. 126.
- Scudder, J. D., and Olbert, S. (1979). A theory of local and global processes which affect solar wind electrons, 1. The origin of typical 1 AU velocity distribution functions—Steady state theory. *J. Geophys. Res.* 84, 2755. doi:10.1029/ja084ia06p02755
- Sheeley, N. R., Lee, D. D.-H., Casto, K. P., Wang, Y.-M., and Rich, N. B. (2009). The structure of streamer blobs. *ApJ* 694, 1471. doi:10.1088/0004-637x/694/2/1471

- Sheeley, N. R., and Rouillard, A. P. (2010). Tracking streamer blobs into the heliosphere. *ApJ* 715, 300. doi:10.1088/0004-637x/715/1/300
- Smith, C. W., and Bieber, J. W. (1991). Solar cycle variation of the interplanetary magnetic field spiral. *Astrophys. J.* 370, 435. doi:10.1086/169830
- Smith, C. W., Acuna, M. H., Burlaga, L. F., L'Heureux, J., Ness, N. F., and Scheifele, J. (1998). The ACE magnetic fields experiment. *Space Sci. Rev.* 86, 611. doi:10.1023/a:1005092216668
- Steinacker, J., and Miller, J. A. (1992). Stochastic gyroresonant electron acceleration in a low-beta plasma. I - interaction with parallel transverse cold plasma waves. *Astrophys. J.* 393, 764. doi:10.1086/171544
- Tang, B., Zank, G. P., and Kolobov, V. (2018). Numerical modeling of electron transport in solar wind: effects of whistler turbulence and Coulomb collisions. *J. Phys. Conf. Ser.* 1100, 012025. doi:10.1088/1742-6596/1100/1/012025
- Trenchi, L., Bruno, R., Telloni, D., D'Amicis, R., Marcucci, M. F., Zurbuchen, T. H., et al. (2013). Solar energetic particle modulations associated with coherent magnetic structures. *Astrophys. J.* 770, 11. doi:10.1088/0004-637x/770/1/11
- Vasko, I. Y., Krasnoselskikh, V., Tong, Y., Bale, S. D., Bonnell, J. W., and Mozer, F. S. (2019). Whistler fan instability driven by strahl electrons in the solar wind. *Astrophys. J. Lett.* 871, L29.
- Versharen, D., Chandran, B. D. G., Jeong, S.-Y., Salem, C. S., Pulupa, M. P., and Bale, S. D. (2019). Self-induced scattering of strahl electrons in the solar wind. *Astrophys. J.* 886, 136. doi:10.3847/1538-4357/ab4c30
- Veselovsky, I. S., Lukashenko, A. T., and Kaportseva, K. B. (2018). Classification scheme for solar wind. *Phys. Atom. Nuclei* 81, 766. doi:10.1134/s1063778818050186
- Viall, N. M., and Borovsky, J. E. (2020). Nine outstanding questions of solar wind physics. *J. Geophys. Res.* 125, e2018JA026005. doi:10.1029/2018ja026005
- Viall, N. M., Kepko, L., and Spence, H. E. (2009). Relative occurrence rates and connection of discrete frequency oscillations in the solar wind density and dayside magnetosphere. *J. Geophys. Res.* 114, A01201. doi:10.1029/2008ja013334
- Viall, N. M., Spence, H. E., Vourlidas, A., and Howard, R. (2010). Examining periodic solar-wind density structures observed in the SECCHI Heliospheric imagers. *Sol. Phys.* 267, 175. doi:10.1007/s11207-010-9633-1
- Viall, N. M., and Vourlidas, A. (2015). Periodic density structures and the origin of the slow solar wind. *Astrophys. J.* 807, 176. doi:10.1088/0004-637x/807/2/176
- Viñas, A. F., Gurgiolo, C., Nieves-Chinchilla, T., Gary, S. P., and Goldstein, M. L. (2010). Whistler waves driven by anisotropic strahl velocity distributions: cluster observations. *AIP Conf. Proc.* 1216, 265. doi:10.1063/1.3395852
- Wang, Y.-M., Sheeley, N. R., Howard, R. A., Rich, N. B., and Lamy, P. L. (1999). Streamer disconnection events observed with the LASCO coronagraph. *Geophys. Res. Lett.* 26, 1349. doi:10.1029/1999gl900177
- Wang, Y.-M., Sheeley, N. R., Socker, D. G., Howard, R. A., and Rich, N. B. (2000). The dynamical nature of coronal streamers. *J. Geophys. Res.* 105, 25113. doi:10.1029/2000ja000149
- Wang, L., Lin, R. P., Krucker, S., and Mason, G. M. (2012). A statistical study of solar electron events over one solar cycle. *Astrophys. J.* 759, 69. doi:10.1088/0004-637x/759/1/69
- Wibberenz, G., and Cane, H. V. (2006). Multi-spacecraft observations of solar flare particles in the inner heliosphere. *Astrophys. J.* 650, 1199. doi:10.1086/506598
- Xu, F., and Borovsky, J. E. (2015). A new four-plasma categorization scheme for the solar wind. *J. Geophys. Res.* 120, 70. doi:10.1002/2014ja020412
- Zhao, L., Zurbuchen, T. H., and Fisk, L. A. (2009). Global distribution of the solar wind during solar cycle 23: ACE observations. *Geophys. Res. Lett.* 36, L14104. doi:10.1029/2009gl039181
- Zhao, L., Landi, E., Kocher, M., Lepri, S. T., Fisk, L. A., and Zurbuchen, T. H. (2016). Anomalously low C^{6+}/C^{5+} ratio in solar wind: ACE/SWICS observation. *AIP Conf. Proc.* 1720, 020006. doi:10.1063/1.4943807

Conflict of Interest: The author declares that the research was conducted in the absence of any commercial or financial relationships that could be construed as a potential conflict of interest.

Copyright © 2021 Borovsky. This is an open-access article distributed under the terms of the Creative Commons Attribution License (CC BY). The use, distribution or reproduction in other forums is permitted, provided the original author(s) and the copyright owner(s) are credited and that the original publication in this journal is cited, in accordance with accepted academic practice. No use, distribution or reproduction is permitted which does not comply with these terms.